Smart Materials and Structures

PAPER

Ionic polymer-metal composite torsional sensor: physics-based modeling and experimental validation

To cite this article: Montassar Aidi Sharif *et al* 2018 *Smart Mater. Struct.* **27** 075039

View the article online for updates and enhancements.

Related content

- A dynamic model for ionic polymer–metal composite sensors
Zheng Chen, Xiaobo Tan, Alexander Will et al.

- A cylindrical ionic polymer-metal composite-based robotic catheter platform: modeling, design and control
Siul Ruiz, Benjamin Mead, Viljar Palmre et al.

- Modelling compression sensing in ionic polymer metal composites
Valentina Volpini, Lorenzo Bardella, Andrea Rodella et al.

This content was downloaded from IP address 35.8.11.2 on 27/06/2018 at 07:13

IOP Publishing Smart Materials and Structures

Smart Mater. Struct. **27** (2018) 075039 (9pp) https://doi.org/10.1088/1361-665X/aac364

Ionic polymer-metal composite torsional sensor: physics-based modeling and experimental validation

Montassar Aidi Sharif[1,2], **Hong Lei**[3], **Mohammed Khalid Al-Rubaiai**[1] and **Xiaobo Tan**[1]

[1] Department of Electrical and Computer Engineering, Michigan State University, East Lansing, MI 48824, United States of America
[2] Department of Computer Engineering, Technical College-Kirkuk, Northern Technological University, Iraq
[3] Schweitzer Engineering Laboratories (SEL), WA, United States of America

E-mail: sharifm5@msu.edu, leihongbuaa@gmail.com, alrubaia@msu.edu and xbtan@egr.msu.edu

Received 2 December 2017, revised 1 May 2018
Accepted for publication 9 May 2018
Published 12 June 2018

Abstract

Ionic polymer-metal composites (IPMCs) have intrinsic sensing and actuation properties. Typical IPMC sensors are in the shape of beams and only respond to stimuli acting along beam-bending directions. Rod or tube-shaped IPMCs have been explored as omnidirectional bending actuators or sensors. In this paper, physics-based modeling is studied for a tubular IPMC sensor under pure torsional stimulus. The Poisson–Nernst–Planck model is used to describe the fundamental physics within the IPMC, where it is hypothesized that the anion concentration is coupled to the sum of shear strains induced by the torsional stimulus. Finite element simulation is conducted to solve for the torsional sensing response, where some of the key parameters are identified based on experimental measurements using an artificial neural network. Additional experimental results suggest that the proposed model is able to capture the torsional sensing dynamics for different amplitudes and rates of the torsional stimulus.

Keywords: ionic polymer-metal composite, IPMC sensor, modeling, physics-based modeling, tubular IPMC, torsional sensor

(Some figures may appear in colour only in the online journal)

1. Introduction

Ionic polymer-metal composites (IPMCs) have built-in sensing and actuation capabilities [1, 2]. In particular, they hold strong promise for versatile applications because they require low-actuation voltages to generate large bending deformation, work in both air and water without stringent packaging requirements, and exhibit direct electromechanical and mechanoelectric transduction, which minimizes the structural complexity in implementation as actuators and sensors [3, 4].

An IPMC typically consists of a thin ion-exchange membrane (e.g., Nafion), chemically plated with a layer of noble metal (e.g., platinum) as electrodes on both surfaces [5, 6]. The traditional fabrication of IPMCs follows the process of impregnation, reduction, and ion-exchange [5]. Inside the polymer, anions are covalently fixed to polymer chains and balanced by cations that can move freely in the membrane. A mechanical deformation on an IPMC sensor breaks this charge balance, leading to the redistribution of the cations and accompanying solvent molecules inside the polymer, as well as the generation of a detectable sensing signal across the electrodes, which can be the open-circuit voltage or short-circuit current. Recent studies on characterization, modeling, and modeling of IPMC can be found in [7–14]. Recent applications of IPMC sensing capability span measurement of displacement [15], flow [16–20], shear loading [21], curvature [22], structural health monitoring [10], and energy harvesting [23–26]. They are also bio-compatible

 © 2018 IOP Publishing Ltd Printed in the UK

and amenable to fabrication [5, 27–31], including 3D-printing [32, 33].

Reported IPMC sensors typically take the shape of beams because thin Nafion films are often used as raw material in the fabrication. Such IPMC sensors only respond to mechanical stimuli acting perpendicular to the beam plane. There have been reports on IPMC actuators or sensors of tubular [34], cylindrical [35], and columnar [36] shapes, which can bend in all directions. A tube-shaped IPMC transducer [37] with patterned outer electrodes was examined by Kim's group through finite element simulations. Its sensing response was experimentally investigated under bending excitation. The buckling effect of IPMC pipes was analyzed by Shen *et al* [38]. Our group previously presented a thin-wall tubular IPMC sensor fabricated with Nafion tubing [39]. The sensor had one common inner electrode and four patterned outer electrodes, and its sensing response under tip-bending excitation was captured with a physics-based model [40].

As discussed above, IPMC sensors, regardless of their shapes, have been mostly studied under bending stimuli. We first reported the effect of torsion sensing for a tubular IPMC device and proposed a preliminary model for describing the sensing behavior in [41], where the charge densities at the inner and outer boundaries were assumed to be proportional to the difference of shear stresses at the two boundaries. While that model showed some agreement in magnitude frequency response with empirical measurement, the match in phase response was less than satisfactory. In particular, the model's phase response shows appreciable positive offset (error) from the empirical data when the frequency is above 4 Hz. Furthermore, since the charge density depends on the densities of both anions and cations, and the (mobile) cation density itself is a state variable that evolves with dynamics, assuming a prescribed charge density at the boundary is unnatural. In this paper, we present an alternative, physics-based modeling approach for the torsional sensing response of an IPMC tube. Compared with [41], this approach not only adopts a more natural assumption, which prescribes the anion concentration in terms of the local shear strain state induced only by the torsion, but also is supported by extensive experimental results that involve transient responses.

In this work the Poisson–Nernst–Planck (PNP) model is adopted to describe the fundamental physics within the IPMC. In particular, the Nernst–Planck equation is used to describe the ionic current inside the polymer, due to cation diffusion, electric field-induced migration, and convection. Poisson's equation is used to describe the electric potential, which affects the cation migration flux. The external torsional stimulus is coupled to the PNP model through the cation convective flux term, where the cation velocity is affected by the solvent pressure, which is related to the polymer pressure caused by the applied mechanical stimulus, as adopted in [37]. A key innovation of the current work is that, we further assume that the anion concentration is perturbed by the local shear strain states induced by the torsion. This is inspired by the assumption used in [37], which relates the *volumetric* strain caused by the bending stimulus to the anion concentration.

Based on the proposed model, time-dependent 3D finite element simulation is conducted for a tubular IPMC sensor under torsional excitation. Experiments are further conducted to compare the sensor response under torsional load with the simulation results, where a novel artificial neural network-based method is used to estimate key parameters of the physical model. The comparison shows that the proposed model is able to capture the sensor behavior under stimuli of different rates and magnitudes. In particular, the model is demonstrated to correctly predict that the sensing current polarity depends only on whether the twist on the sensor is increased or decreased. In comparison, a model relating the volumetric strain to the anion concentration would predict a behavior qualitatively different from the experimental observation.

The remainder of the paper is organized as follows. The physics-based model is discussed in section 2. The fabrication of the IPMC tubular sensor and experimental characterization of its sensing behavior under torsion are presented in section 3. Parameter identification and model validation are presented in section 4. Finally, concluding remarks and future work are provided in section 5.

2. Physics-based modeling of the tubular IPMC sensor under torsion

The transport of cations within the IPMC under applied loads is governed by the Nernst–Planck equation (NP) and the electrical potential is related to the charge density via Poisson's equation (P). These two equations, collectively known as the PNP equations, along with appropriate coupling relating the mechanical stimulus to the charge density, provide a physical model for the IPMC sensor. Much of our model development and finite element modeling implementation follows the approach in [37] for the case of an omnidirectional *bending* sensor; however, there is a key difference in terms of how the external mechanical stimulus (torsion versus bending) is incorporated into the model.

2.1. PNP Model

For an IPMC sensor subjected to an external mechanical load, the induced ion movement leads to the redistribution of the charge density. The transport of cations is governed by the NP equation [35]. The flux vector J of cations consists of terms from diffusion, electromigration, and convection:

$$J = \underbrace{-D\nabla C^+}_{Diffusion} - \underbrace{zD\frac{1}{RT}FC^+\nabla\phi}_{Electromigration} - \underbrace{D\frac{1}{RT}C^+\Delta V\nabla P}_{Convection}, \quad (1)$$

where C^+ is the cation concentration, z is the charge number of the cation, D is the diffusion coefficient, R is the gas constant, T is the absolute temperature, F denotes Faraday's constant, ϕ is the electric potential, ΔV is the molar volumetric change, which represents how much the polymer volume swells after taking water, and ∇P is the solvent pressure gradient. As treated in [37], the solvent pressure gradient is considered to be balanced by the gradient of the polymer pressure, ∇p,

$$\nabla P = -\nabla p, \tag{2}$$

where p is the average normal stress of the polymer, resulting from solid mechanics calculation subject to the external load.

From the continuity equation

$$\frac{\partial C^{+}}{\partial t} = -\nabla \cdot J, \tag{3}$$

where '$\nabla\cdot$' denotes the divergence, one gets the NP equation:

$$\frac{\partial C^{+}}{\partial t} + \nabla \cdot (-D\nabla C^{+} - z\frac{D}{RT}FC^{+}\nabla\phi \\ -\frac{D}{RT}C^{+}\Delta V\nabla P) = 0. \tag{4}$$

The electric potential inside the polymer is related to the charge density ρ

$$\nabla^2\phi = -\frac{\rho}{\kappa_e}, \tag{5}$$

where '∇^2' denotes the Laplace operator, and κ_e is the effective dielectric constant of the polymer. The charge density is related to the ionic concentrations as follows:

$$\rho = F(C^{+} - C^{-}), \tag{6}$$

where C^{-} is the local anion concentration, which is considered to be related to the local shape change under the applied torsional excitation, as discussed next.

2.2. Mechano-electrical coupling

The anion concentration C^{-} can be related to the local deformation induced by the mechanical stimulus. This was first done in [37], where the authors relate C^{-} to the local volume change (approximated by the divergence of local displacement $\nabla \cdot u$) under a bending stimulus

$$C^{-} = C_0(1 - \nabla \cdot u), \tag{7}$$

where C_0 represents the nominal anion concentration in the absence of deformation, and $u = (u_1, u_2, u_3)^T$ represents the displacement along x, y, and z directions, respectively. For a tube under pure torsion, $\nabla \cdot u = 0$, thus there would be no change in C^{-} under (7). Since the displacement under torsion is induced by shear, we propose instead

$$C^{-} = C_0(1 - \gamma), \tag{8}$$

where γ is the sum of the shear strains [42]:

$$\gamma = \epsilon_{xy} + \epsilon_{yz} + \epsilon_{zx}. \tag{9}$$

Figure 1. Fabricated tubular IPMC sensor.

3. Sensor fabrication and experimental characterization

3.1. Fabrication of tubular IPMC Sensors

The fabrication of tubular IPMC sensors generally follows the traditional impregnation, reduction, and ion-exchange process [40]. The Nafion tubing (TT-110, Perma Pure LLC) was used as the raw material, which had an inner diameter of 2.4 mm, outer diameter of 2.93 mm, and wall thickness of 265 μm. It was first rinsed with acetone then methanol to clean the tubing and to ensure that the surfaces of the sensor were free from impurities that might affect the fabrication process. Then the Nafion tubing was boiled in dilute hydrochloric acid (2 wt%) for 30 min to remove impurities, and then boiled in deionized (DI) water for another 30 min to remove the acid and swell the film. After these pre-treatment steps, the Nafion tubing was immersed in a platinum complex solution ($[Pt(NH_3)_4]Cl_2$) for more than 4 h (usually 4–8 h) to allow platinum ions to diffuse into the Nafion polymer completely through the ion-exchange process. After a rinse with DI water, the tubing was immersed in a water bath at 40 °C for 30 min. After the temperature was raised to 60 °C, a sodium borohydride solution (5 wt% $NaBH_4$ aq) was added to the water bath as a reducing agent at a rate of 2 ml every 30 min. Once the platinum deposition was complete, those steps were repeated, from acid treatment to water bath reduction, to deposit the platinum for the second time. The tubing was then boiled in DI water for one hour to release the internal stress. After that, it was put into a sodium chloride solution to exchange the residual platinum ions with sodium ions. The tubing was then cut into segments of desired lengths. Finally, a tubular IPMC sensor was formed by attaching two wire connectors to the inner and outer surfaces of the IPMC, respectively. Figure 1 shows the pictures of a fabricated tubular IPMC sensor.

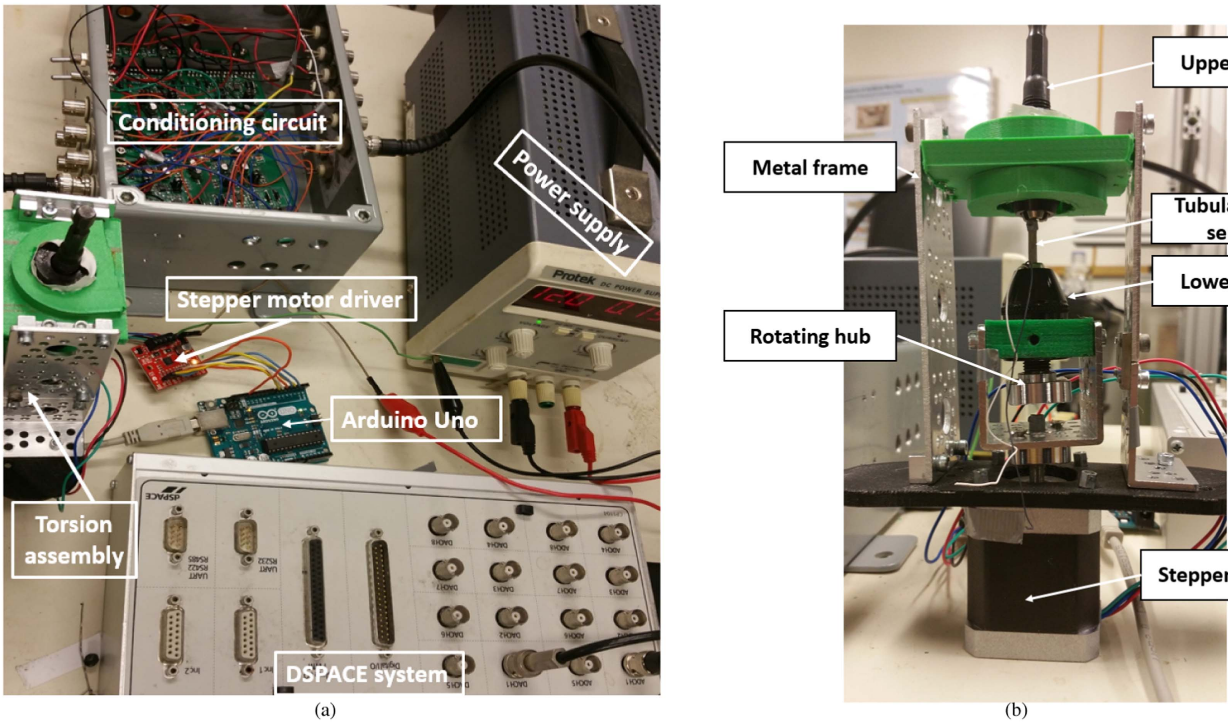

(a) (b)

Figure 2. (a) Experimental setup involving the torsion assembly, conditioning circuit for the sensing output, and dSPACE system for data acquisition; (b) details of the torsion assembly.

3.2. Experimental setup

To characterize the sensor behavior under torsional excitation, we impose a pure torsional load at the tip of the tubular IPMC sensor. The short-circuit current between the inner and outer electrodes is taken as the sensor output. Figure 2(a) shows the major elements of the setup, including the torsion assembly that imposes a torsional load on the IPMC tubular sensor, the conditioning circuit [43] that filters and amplifies the sensing output, and the dSPACE system (RTI 1104) for data acquisition. Figure 2(b) shows the details of the torsion assembly. The tubular IPMC sensor is fixed with two drill chucks, one on each end. The chucks securely hold the sensor and ensure no slip when a torsional load is applied. The top end of the IPMC sensor is fixed on a 3D-printed plate, which is rigidly connected to a metal frame. The lower chuck is attached to a stepper motor (SparkFun Electronics—ROB 10846) which is used to generate a programmed angle of twist on the lower end of the IPMC. The stepper motor is controlled via a microcontroller (Arduino-uno).

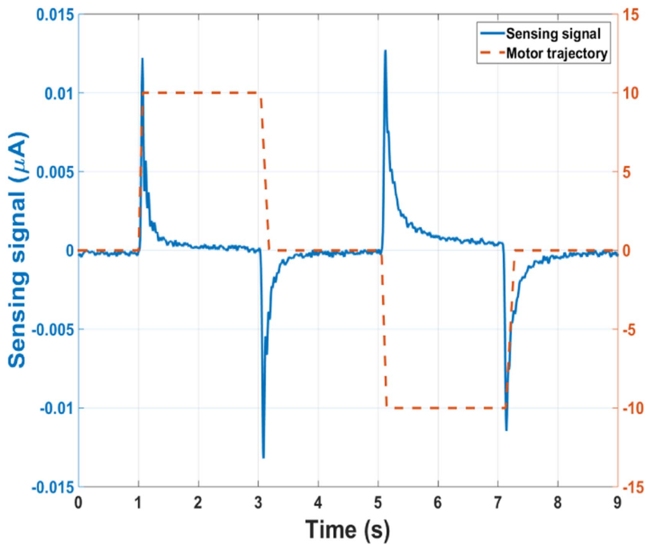

Figure 3. The applied sequence of motor inputs in loading/unloading the torsion, first in one direction and then in the other, and the corresponding sensing signal. Here the motor speed in ramping up/down is $360^\circ\ s^{-1}$ and the twist angle magnitude is 10°.

3.3. Sensor characterization

The responses of the tubular IPMC sensor are characterized with a sequence of torsional stimuli, to examine both its transient and steady state behaviors. In particular, the angle of the stepper motor first ramps up from 0° to an angle θ in the clockwise direction, holds for 2 s, and then ramps back down to 0°; it then holds for 2 s, ramps up to θ in the counter-clockwise direction, holds for 2 s, and finally ramps back down to 0°. Figure 3 shows an example of the motor trajectory, where θ is 10°, and the speed of the motor when ramping up and down is $360^\circ\ s^{-1}$. We note that the chosen sequence of the motor movement allows us to examine a number of sensor behaviors, including both the dynamic behavior during transients and the steady state behavior (when the torsion angle is held constant for 2 s), the polarity of the sensing current during loading/unloading of the torsional stimulus, and the polarity of the sensing output when the sensor is twisted in one direction versus the other. Figure 3 also shows the short-circuit current response from the sensor under the

Table 1. Model parameters.

F (C mol^{-1})	R (J mol^{-1} K^{-1})	T (K)	z	σ (S m^{-1})
96 487	8.3143	290	1	7000.1
D (m^2 s^{-1})	C_0 (mol m^{-3})	ϵ (F m^{-1})	ρ (kg m^{-3})	E (Pa)
3.2×10^{-11}	1056	5×10^{-3}	2130	3.4×10^8

corresponding motor input. It can be seen that, when the torsion is loaded or unloaded, the sensor current produces a spike, which then approaches zero at the steady state. Furthermore, the polarities of the spikes during loading and unloading are opposite, and the polarity is independent of the loading orientation (clockwise or counterclockwise). These rich behaviors offer good tests for the proposed model. In addition, as will be discussed in section 4, the model will be further tested by examining its ability to predict the sensor responses under different loading/unloading speeds and magnitudes.

4. Parameter identification and model validation

4.1. Parameter identification

Parameters for the model proposed in section 2 are determined and used in model validation. The sensor dimensions, including the length, the inner and outer diameters, and the thickness of the platinum electrode layers, are obtained directly through measurement. In particular, the thickness of the platinum layers is computed using the measured thickness of the polymer tubing before fabrication and that of the fabricated IPMC tube. For the tubular IPMC sensor used in experiments, the dimensions are: length 15 mm, inner diameter 2.31 mm, outer diameter 3.02 mm. The physical constants in the model include the temperature (T), which is measured directly using a thermometer, density (ρ), which is obtained through measuring the sensor weight and volume, the Faraday constant (F), and the gas constant (R). The value of anion concentration C_0 was taken from [40]. The electrical conductivity of the electrode (σ) was determined with the measured sensor surface resistance and the dimensions of the electrode. Table 1 lists the aforementioned parameters and constants.

The remaining parameters include the Young's modulus Y, diffusion coefficient D, and dielectric constant ϵ, all of which are obtained through an artificial neural network-based data fitting process. The Matlab toolbox (*nnstart*) is used to prepare a neural network with three inputs, which represent the parameters to be tuned, and one output, which represents the model fitting error. We have used a multilayer perceptron (MLP) network that contains one hidden layer with 10 nodes. The number of hidden layers and nodes are chosen according to [44]. Specifically, we use the imposed motor angle trajectory and the corresponding sensing signal in the first two seconds of the experiment shown in figure 3, for the purpose of parameter identification, and these same parameters will be used in other scenarios (different loading/unloading magnitudes and rates) of the experiments for model validation. Since the proposed model for the torsion sensor does not have an analytical input–output relationship expressed in terms of the parameters, finite element simulation is used to obtain the predicted sensing signal trajectory for the prescribed torsion stimulus, for any given set of parameters.

The simulation of tubular IPMC sensor model under torsional excitation, as described in section 2, is implemented with COMSOL Multiphysics 5.1 finite element software packages. Four physics packages are used to implement the sensor model: solid mechanics, transport of diluted species, general-form PDE to generate the electrical potential within the nafion, and electrical current physics. The solid mechanics module is used to describe the linear elastic material under torsional excitation. The PNP model, which is used to describe the electrical potential and the cation concentration inside the Nafion during the deformation, is realized through the transport of diluted species physics and the general-form PDE physics. The implementation of the IPMC model under torsional stimuli is achieved with two separate computations. The deformation of the IPMC sensor is calculated first, followed by the execution of the PNP model, which uses the deformation data from the first study computation as input. A short-circuit current is collected by imposing the electrodes with zero potential and integrating the collected current density throughout the electrode surface.

We follow a tutorial provided by Matlab Inc. [45] to implement the neural network model, which offers a step-by-step instruction on how to use the command (*nnstart*). The neural network model requires a number of input–output data sets to start the training. In addition, the neural network needs to dedicate some of the input–output sets to test and validate the network after the training is completed. The average error between the predicted and measured sensing signals is treated as the output of the neural network for the corresponding input values (i.e., the parameters used in the simulation). A total of 120 sets of parameters, chosen within feasible ranges of these parameters, are used in conducting the simulation. Ninety sets of the obtained input–output data are used to train the neural network, 10 sets are used to test the neural network (cross validation), while 20 sets are used to validate the obtained neural network mode. An overall match of 98% is achieved between the trained neural network model and the experimental data. The 98% match is used as stopping criterion to stop the training process which is the highest matching we get in this process. The established neural network model is then used to serve as a fitness function to the optimization toolbox (*optimtool*) to find the optimal input vector that minimizes the output, which produces the optimal parameters (Y, D, ϵ) for the data fitting. The obtained values for these parameters are also listed in table 1. Figure 4 shows the comparison between measured signal and the model prediction based on the identified parameters. It can be seen that overall the model captures well the magnitude and transient behavior of the sensing response under the given stimulus.

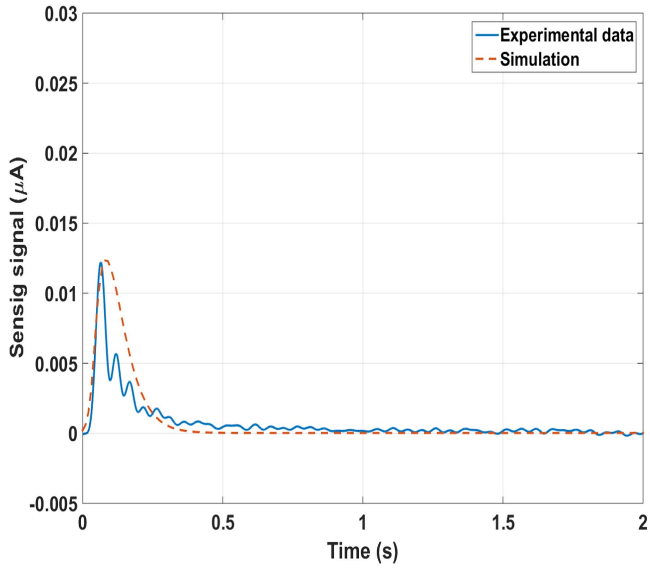

Figure 4. Testing results: a comparison between the experimental measurement and the simulation model after applying 10° twisting angle.

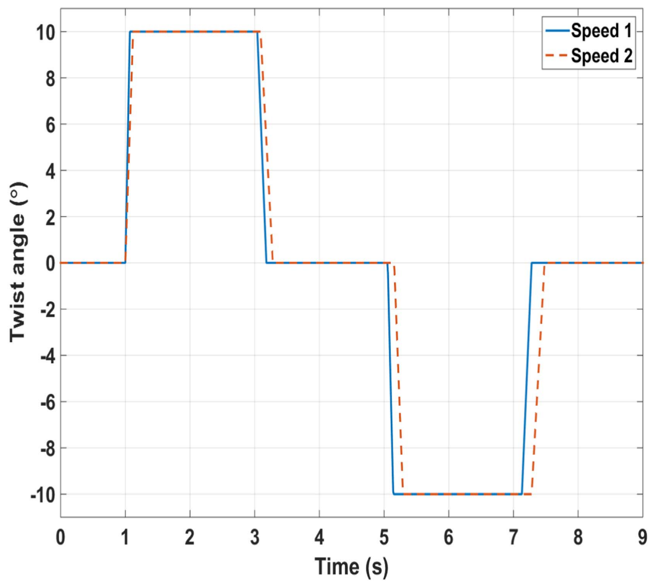

Figure 5. Input trajectory: two different stepper motor speeds to reach a specific angle.

4.2. Model validation

The identified parameters are then used in the simulation of the sensor responses under torsional stimuli of different magnitudes (10°, 15°, 20°) and loading/unloading rates. In particular, two loading/unloading speeds, $360^\circ\ s^{-1}$ and $180^\circ\ s^{-1}$, are adopted; figure 5 illustrates the profiles of the two speeds.

Figures 6(a)–(f) show the comparison between the measured sensor outputs and the model-predicted sensor outputs under different stimuli. Overall, all figures show good agreement between the measurement and model prediction. Given that three of the key model parameters are identified using only part of the data under a particular torsional stimulus, the reasonable match across all cases provides strong support for the validity of the model. Specifically, the model is able to capture the magnitude, transients, and polarity of the sensor response. For example, the polarity of the sensing signal is determined only by the loading or unloading trend of the stimulus, instead of the orientation of the torsional stimulus. The model also predicts correctly that the sensor response converges to zero at the steady state (for a constant torsion input). For the same loading rate, the results show that the sensing output magnitude increases with the stimulus magnitude (for example, see figures 6(a), (c), and (e)). For the same stimulus magnitude, a higher loading/unloading rate results in higher sensing response (for example, see figures 6(a) and (b)).

Despite the general good agreement, there are some modest discrepancies between the experimental data and the simulation results, which we attribute mainly to the imperfection in the fabrication of the tubular IPMC sensor and in the experimental setup. This can be seen, for example, in the experimental curve in figure 6(c). The two positive signal spikes, ideally, should be identical; however, the transient speed of the second spike is appreciably slower than the first one, which can be seen from the increased offset between the simulated curve and the experimental curve for the second peak. A similar observation can be made for the two negative signal spikes. The latter could be caused by the rotation asymmetry between clockwise and counterclockwise directions. If one focuses on the first half of each subfigure, the agreement between the experimental data and model prediction is much more consistent.

Finally, to demonstrate the unique utility of the proposed model, we simulate the sensor response using the model in [37] for a torsional stimulus of magnitude 10° and rate $360^\circ\ s^{-1}$. Recall that the key difference between the proposed model and the model in [37] is that the latter relates the volumetric strain to the local anion concentration. From figure 7, it can be seen that the model in [37], which was shown to work well for a bending sensor, cannot capture the qualitative behavior of the tubular IPMC sensor under torsion. In particular, it fails to correctly capture the polarity of the sensing response as observed in experiments. It also predicts asymmetric positive and negative responses, which are not observed in experiments.

5. Conclusions

In this paper we reported a new physics-based model for a tubular IPMC sensor subjected to a torsional load. The model was built upon the PNP equations for capturing the movement of cations. A key innovation of this work was the proposal of relating the shear strains to the local anion concentration. An experimental setup was created for applying twist at one end of the IPMC tube while keeping the other end fixed. Experiments involving stimuli of different magnitudes, loading orientations, and loading/unloading speeds were conducted, and the proposed model was shown to be able to capture the trends observed experimentally.

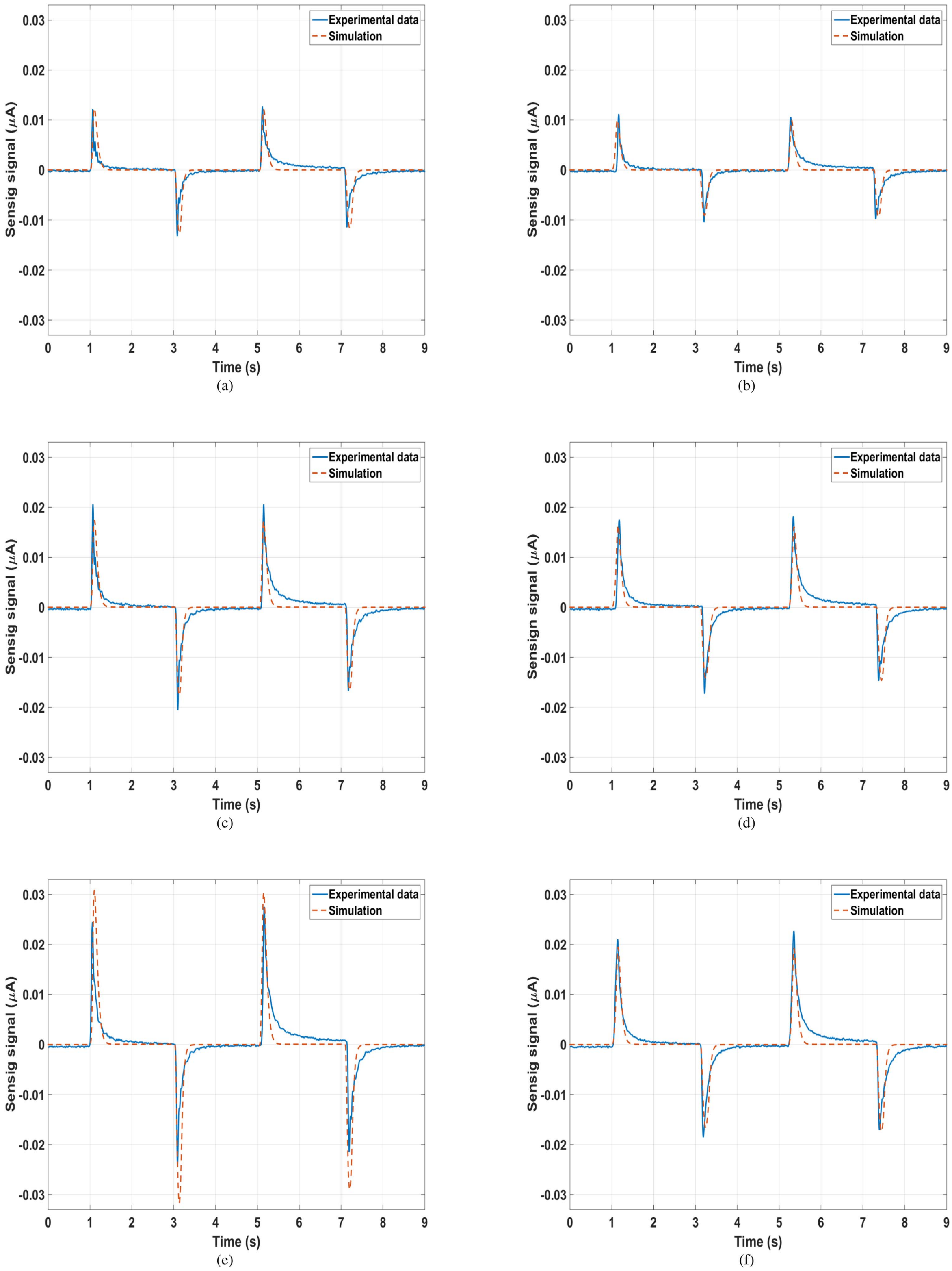

Figure 6. Comparison between the experimental measurement and model prediction of the sensor response under different torsional stimuli: (a) torsion magnitude 10°, speed 360° s^{-1}; (b) torsion magnitude 10°, speed 180° s^{-1}; (c) torsion magnitude 15°, speed 360° s^{-1}; (d) torsion magnitude 15°, speed 180° s^{-1}; (e) torsion magnitude 20°, speed 360° s^{-1}; (f) torsion magnitude 20°, speed 180° s^{-1}.

For future work, we will explore the use of the tubular IPMC sensor in practical applications, such as measuring torque and angular acceleration and providing feedback for control. For those applications, it will be of interest to reduce the proposed physics-based model to a low-dimensional model that is amenable to signal processing (for example, decoding the stimulus based on the sensor output) and feedback control design.

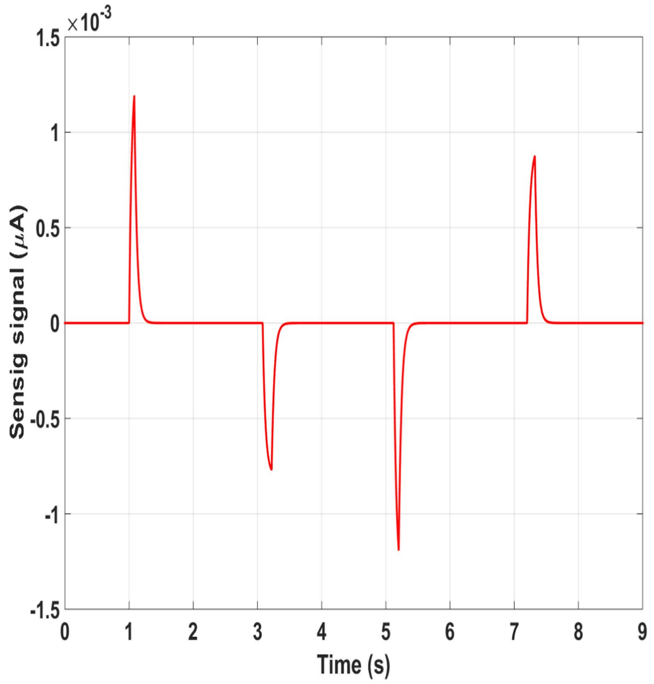

Figure 7. The simulated sensing response when the model in [37] is adopted for the stimulus of magnitude of 10° and rate of 360° s^{-1}.

Acknowledgments

This work was supported in part by National Science Foundation (DBI 0939454) and the Office of Naval Research (N000141210149, N000141512246). The work of Sharif was also supported by the Higher Committee for Education Development in Iraq (HCED).

ORCID iDs

Montassar Aidi Sharif https://orcid.org/0000-0002-9879-0631
Xiaobo Tan https://orcid.org/0000-0002-5542-6266

References

[1] Bar-Cohen Y 2004 *Electroactive Polymer (EAP) Actuators as Artificial Muscles: Reality, Potential and Challenges* (Bellingham, WA: SPIE Press)

[2] Shahinpoor M and Kim K 2001 Ionic polymer-metal composites: I. Fundamentals *Smart Mater. Struct.* **10** 819–33

[3] Shahinpoor M, Bar-Cohen Y, Simpson J and Smith J 1998 Ionic polymer-metal composites (IPMCs) as biomimetic sensors, actuators and artificial muscles—a review *Smart Mater. Struct.* **7** R15–30

[4] Shahinpoor M and Mojarrad M 2002 Ionic polymer sensors and actuators *US Patent* No. 6475639

[5] Kim K J and Shahinpoor M 2003 Ionic polymer-metal composites: II. Manufacturing techniques *Smart Mater. Struct.* **15** 65–79

[6] Palmre V, Pugal D, Kim K J, Leang K K, Asaka K and Aabloo A 2014 Nanothorn electrodes for ionic polymer-metal composite artificial muscles *Sci. Rep.* **4** 6176

[7] Cha Y, Aureli M and Porfiri M 2012 A physics-based model of the electrical impedance of ionic polymer metal composites *J. Appl. Phys.* **111** 124901

[8] Lei H, Lim C and Tan X 2015 Humidity-dependence of IPMC sensing dynamics: characterization and modeling from a physical perspective *Meccanica* **50** 2663–73

[9] Sun Z, Hao L, Chen W, Li Z and Liu L 2013 A novel discrete adaptive sliding-mode-like control method for ionic polymer-metal composite manipulators *Smart Mater. Struct.* **22** 095027

[10] Lei H, Lim C and Tan X 2013 Modeling and inverse compensation of dynamics of base-excited ionic polymer-metal composite sensors *J. Intell. Mater. Syst. Struct.* **24** 1557–71

[11] Xiong Y, Chen Y, Sun Z, Hao L and Dong J 2014 Active disturbance rejection control for output force creep characteristics of ionic polymer metal composites *Smart Mater. Struct.* **23** 075014

[12] Aureli M and Porfiri M 2013 Nonlinear sensing of ionic polymer metal composites *Contin. Mech. Thermodyn.* **25** 273–310

[13] Hao L and Li Z 2010 Modeling and adaptive inverse control of hysteresis and creep in ionic polymer-metal composite actuators *Smart Mater. Struct.* **19** 025014

[14] Farinholt K and Leo D J 2004 Modeling of electromechanical charge sensing in ionic polymer transducers *Mech. Mater.* **36** 421–33

[15] Dong R and Tan Y 2015 A model based predictive compensation for ionic polymer metal composite sensors for displacement measurement *Sensors Actuators* A **224** 43–9

[16] DeVries L, Lagor F D, Lei H, Tan X and Paley D A 2015 Distributed flow estimation and closed-loop control of an underwater vehicle with a multi-modal artificial lateral line *Bioinsp. Biomim.* **10** 025002

[17] Zhang F, Lagor F D, Lei H, Tan X and Paley D A 2016 Robotic fish: flow-relative control behaviors using distributed flow sensing *Mech. Eng.* **138** S2

[18] Ahrari A, Lei H, Sharif M A, Deb K and Tan X 2017 Design optimization of an artificial lateral line system incorporating flow and sensor uncertainties *Eng. Optim.* **49** 328–44

[19] Ahrari A, Lei H, Sharif M A, Deb K and Tan X 2017 Reliable underwater dipole source characterization in 3d space by an optimally designed artificial lateral line system *Bioinsp. Biomim.* **12** 036010

[20] Lei H, Sharif M A, Paley D A, McHenry M J and Tan X 2016 Performance improvement of IPMC flow sensors with a biologically-inspired cupula structure *Electroactive Polymer Actuators and Devices (EAPAD) 2016* vol 9798 (International Society for Optics and Photonics) p 979827

[21] Zangrilli U and Weiland L 2011 Prediction of the ionic polymer transducer sensing of shear loading *Smart Mater. Struct.* **20** 094013

[22] Bahramzadeh Y and Shahinpoor M 2011 Dynamic curvature sensing employing ionic-polymer-metal composite sensors *Smart Mater. Struct.* **20** 094011

[23] Cellini F, Intartaglia C, Soria L and Porfiri M 2014 Effect of hydrodynamic interaction on energy harvesting in arrays of ionic polymer metal composites vibrating in a viscous fluid *Smart Mater. Struct.* **23** 045015

[24] Cha Y, Verotti M, Walcott H, Peterson S D and Porfiri M 2013 Energy harvesting from the tail beating of a carangiform swimmer using ionic polymer metal composites *Bioinsp. Biomim.* **8** 036003

[25] Cha Y, Shen L and Porfiri M 2013 Energy harvesting from underwater torsional vibrations of a patterned ionic polymer metal composite *Smart Mater. Struct.* **22** 055027

[26] Peterson S D and Porfiri M 2012 Energy exchange between a vortex ring and an ionic polymer metal composite *Appl. Phys. Lett.* **100** 114102

[27] Hao L N, Chen Y and Zhao Y S 2015 Research on enhanced performance of ionic polymer metal composite by multiwalled carbon nanotubes *Mater. Res. Innov.* **19** 477–81

[28] Lei H, Li W and Tan X 2012 Microfabrication of IPMC cilia for bio-inspired flow sensing *Proc. SPIE* **8340** 83401A

[29] Lei H, Li W and Tan X 2014 Encapsulation of ionic polymer-metal composite (IPMC) sensors with thick parylene: fabrication process and characterization results *Sensors Actuators* A **217** 1–12

[30] Sareh S, Rossiter J, Conn A, Drescher K and Goldstein R E 2013 Swimming like algae: biomimetic soft artificial cilia *J. R. Soc. Interface* **100** 20120666

[31] Sivasubramanian B and Kim D 2014 Development, analysis, and comparison of electromechanical properties of buckypaper IPMC actuator *Proc. SPIE* **9056** 2045287

[32] Carrico J D, Traeden N W, Aureli M and Leang K K 2015 Fused filament 3d printing of ionic polymer-metal composites (IPMCs) *Smart Mater. Struct.* **24** 125021

[33] Carrico J D and Leang K K 2017 Fused filament 3d printing of ionic polymer-metal composites for soft robotics *Electroactive Polymer Actuators and Devices (EAPAD) 2017* vol 10163 (International Society for Optics and Photonics) p 101630I

[34] Oguro K, Fujiwara N, Asaka K, Onishi K and Sewa S 1999 Polymer electrolyte actuator with gold electrodes *Proc. SPIE* **3669** 3669–39

[35] Kim S J, Pugal D, Wong J, Kim K J and Yim W 2014 A bio-inspired multi degree of freedom actuator based on a novel cylindrical ionic polymer-metal composite material *Robot. Auton. Syst.* **62** 53–60

[36] Lei H and Tan X 2013 Fabrication and characterization of a two-dimensional IPMC sensor *Proc. SPIE* **8687** 868707

[37] Stalbaum T, Pugal D, Nelson S E, Palmre V and Kim K J 2015 Physics-based modeling of mechano-electric transduction of tube-shaped ionic polymer-metal composite *J. Appl. Phys.* **117** 114903

[38] Shen L, Cha Y, Shams A and Porfiri M 2013 Fabrication and buckling analysis of ionic polymer metal composite pipes *Smart Mater. Struct.* **22** 105032

[39] Lei H and Tan X 2014 A novel tubular thin-wall IPMC sensor capable of two-dimensional sensing: fabrication, characterization and modeling *Proc. ASME 2014 Conf. on Smart Materials, Adaptive Structures and Intelligent Systems* (Newport, RI: ASME) pp SMASIS2014–7594

[40] Lei H, Sharif M A and Tan X 2016 Dynamics of omnidirectional IPMC sensor: experimental characterization and physical modeling *IEEE/ASME Trans. Mechatronics* **21** 601–12

[41] Lei H, Sharif M A and Tan X 2016 A dynamic physics-based model for tubular IPMC sensors under torsional excitation *Proc. SPIE* **9798** 979836

[42] Gurtin M E 1973 The linear theory of elasticity *Linear Theories of Elasticity and Thermoelasticity* (Berlin: Springer) pp 1–295

[43] Ganley T, Hung D L, Zhu G and Tan X 2011 Modeling and inverse compensation of temperature-dependent ionic polymer-metal composite sensor dynamics *IEEE/ASME Trans. Mechatronics* **16** 80–9

[44] Stathakis D 2009 How many hidden layers and nodes? *Int. J. Remote Sens.* **30** 2133–47

[45] 2014 *Fit Data with a Neural Network, Tutorial (R2014b)* (Natick, MA: The Mathworks, Inc.)